

Anisotropic Electron-Phonon Coupling Uncovered By Angle-Resolved Photoemission

T.P.D evereaux,^a T.C uk,^b Z.-X .Shen,^b and N .N agaosa^c

^aDepartment of Physics, University of Waterloo, Waterloo, Ontario, N2L 3G1, Canada

^bDept. of Physics, Applied Physics and Stanford Synchrotron Radiation Laboratory, Stanford University, California 94305, USA

^cDepartment of Applied Physics, University of Tokyo, Bunkyo-ku, Tokyo 113-8656, Japan

Abstract

Recently there has been an accumulation of experimental evidence in the high temperature superconductors suggesting the relevance of electron-phonon coupling in these materials. These findings challenge some well-held beliefs of what electron-phonon interactions can and cannot do. In this article we review evidence primarily from angle-resolved photoemission (ARPES) measurements which point out the importance of electronic coupling to certain phonon modes in the cuprates.

Key words: Angle-resolved Photoemission, Electron-Phonon Coupling, Collective Modes.

The physics underlying the peculiar behavior of the high temperature superconductors in the normal state and the high transition temperatures themselves is far from understood. While the importance of magnetic interactions has been widely pointed out, a number of experimental findings strongly suggest that electron-phonon coupling must play a role in these materials. These findings include strong phonon renormalizations with temperature and/or doping seen in neutron and Raman scattering[1,2], the doping dependence of the isotope effect of the transition temperature[3], the isotope dependence of the superfluid density[4], and lastly the pressure, layer and material dependence of T_c itself.

In this paper we focus attention on some recent developments coming from angle-resolved photoemission (ARPES) experiments and theoretical developments of anisotropic electron-phonon interactions in general.

Initially, the attention to bosonic renormalization effects in cuprate superconductors was focussed on a "kink" in the electronic dispersion near 50-70 meV for nodal electrons[5,6,7,8,9] or solely below

T_c [8,10,11,12]. This has been further shown to be generic to many hole-doped cuprates and is seen both in the normal and superconducting states[13]. Recently, the "kink" phenomenon has been reported for electronic states throughout the Brillouin zone (BZ) again both above and below T_c [13]. Although many-body effects reminiscent of strong coupling are known to exist below T_c in an extended k -space range, the observation of kinks in the normal state imposes an additional constraint. In contrast to the nodal renormalization which shows little change across T_c , data in the anti-nodal region reveal a dramatic change in the effective coupling through T_c [13], as shown in Fig. 1 for $\text{Bi}_2\text{Sr}_2\text{Ca}_{0.92}\text{Y}_{0.08}\text{Cu}_2\text{O}_{8+}$ (Bi-2212). In the superconducting state, classical Engelsberg-Schrieffer signatures of electronic coupling to a bosonic mode are seen in the image plot. The image plot shows strong "kinks" or breaks in the energy dispersion of the band near the $(\pi;0)$ regions of the BZ, and weaker kinks near the nodal directions. The shift in the energy at which the 40 meV mode couples to the electrons (< 30 deg) compounded by the lack of shift in the 60-70 meV nodal kink (> 35 deg) gives rise to a fairly uniform 65-70 meV kink energy throughout

Corresponding Author Email: tpd@lorax.uwaterloo.ca

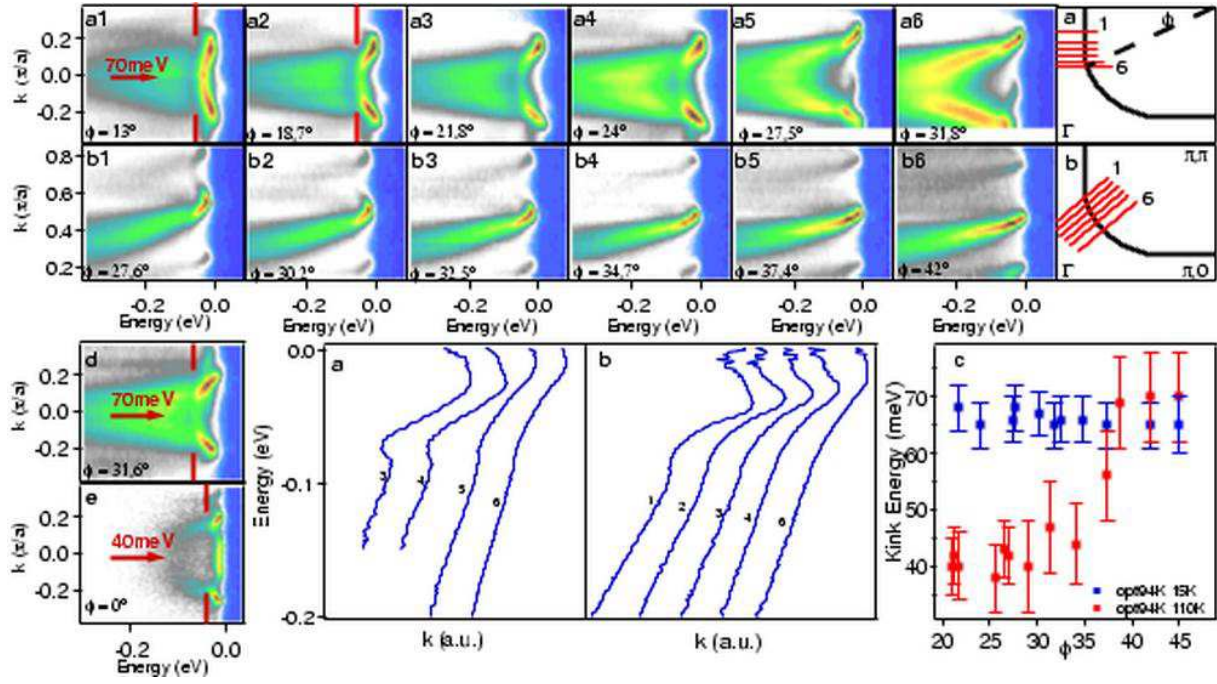


Fig. 1. The image plots in a1-a6), and the corresponding MDC-derived dispersions, are cuts taken parallel to $(0; -)$ ($;$) at the locations indicated in the sketched zone at 15K. The image plots in b1-b6), and the corresponding MDC-derived dispersions, are cuts taken parallel to $(0; 0)$ ($;$), at k-space locations indicated in the zone at 15K. Kink energies as a function of angle are summarized in c) for optimally (94K) doped samples in the normal and superconducting states. d) and e) are spectra taken parallel to $(0; -)$ ($;$) at the k-space locations indicated for under-doped (85K) and over-doped samples (65K) of Bi-2212, respectively.

the BZ in the superconducting state. The coupling strength, on the other hand, has a strong momentum dependence below T_c . The relative sharpness of the Momentum Distribution Curves (MDC) kink (Fig. 1(a,b)) indicates that the effective coupling strength increases from the node to the antinode of the d-wave gap. One can also see the increase in coupling in the image plots of the raw data towards $(\pi; 0)$ as there is a stronger depression in intensity at the mode energy. When the coupling gets very strong as in Fig. 1(a1,a2), little dispersion can be tracked, and this is the primary indicator of coupling. The kinks occur for different dopings, and are clearly seen in underdoped as well as overdoped samples, as shown in Figure 1d,e, respectively. In the deeply overdoped sample ($T_c = 65K$ or $\sim 22\%$), Fig. 1e, the kink energy moves to 40-45 meV since ϵ_0 (10-15 meV) becomes much smaller. In the underdoped sample ($T_c = 85K$), Fig. 1d, the kink energy remains around 70 meV since it has a similar gap as the optimally doped sample ($\epsilon_0 = 35-40$ meV). The signatures of coupling remain strong throughout, although they do noticeably increase from the overdoped to underdoped sample when comparing data taken at the same ϕ .

In the normal state little of these effects can be seen without further analysis. As a consequence, kinks in

the normal state have been missed in prior works. In Fig. 2, we have extracted dispersions for three k-space cuts in a momentum space region between the nodal direction and the Van Hove Singularity (VHS) at $(\pi, 0)$. Since we are only concerned with the energy scale, we plot the energy dispersion curves (EDCs) phenomenologically. The usual method to extract dispersions [fitting MDC with Lorentzians] is not appropriate since the assumed linear approximation of the bare band fails towards $(\pi, 0)$ where the band bottom is close to E_F [14]. EDC-derived dispersions of three independent data sets shown in Fig. 2 consistently reveal a 40 meV energy scale in the normal state (a1,b1,c), evolving into a 70 meV feature in the superconducting state (a2,b2), as summarized in Figure 2d. In the superconducting state where the coupling is strongest, the peak position in both EDC and MDC dispersions asymptotically approach the characteristic energy defined by the bosonic mode (Fig. 2a2, Fig. 2b2).

The kink energy shift is due to the opening of a superconducting gap which shifts the energy at which the electronic states couple to the bosonic mode. Here, we observe a kink shift of $\sim 25-30$ meV, close to the maximum gap energy, 40 meV. We summarize the temperature dependence of the energy at which we see a bosonic mode couple to the electronic states in the anti-nodal

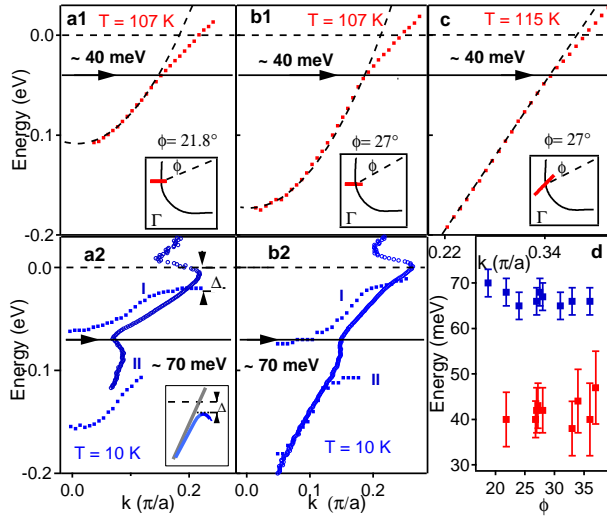


Fig. 2. EDC (a1, b1, c) derived dispersions in the normal state (107 K and 115 K). and the cut-direction are noted in the insets. The red dots are the data; the fit to the curve (dashes, black) below the 40 meV line is a guide to the eye. a2) and b2) are MDC derived dispersions at the same location and direction as in a1) and b1), but in the superconducting state (15 K). In a2) and b2) we also plot the peak (I) and hump positions (II) of the EDCs for comparison. The inset of a2) shows the expected behavior of a Bogoliubov type gap opening. The S-like shape below the gap energy is an artifact of how the MDC handles the back-bend of the Bogoliubov quasiparticle. d) kink positions as a function of ϕ in the anti-nodal region.

region in Figs. 1 (c) and 2 (d): the kink energies are at 40 meV above T_c near the anti-nodal region and increase to 70 meV below T_c . Because the band minimum is too close to E_F , the normal state 40 meV kink cannot easily be seen below 20° .

By comparing the different cut directions, one can clearly see that the coupling is extended in the Brillouin zone and has a similar energy scale throughout, near 70 meV. Moreover, the signatures of coupling increase significantly toward $(\pi, 0)$ or smaller ϕ . The clear minimum in spectral weight seen near 70 meV in Fig. 2a1) and 2a2) indicates strong mixing of the electronic states with the bosonic mode where the two bare dispersions coincide in energy.

The above described experimental observations are difficult to reconcile in the spin resonance mode scenario. The kink is clearly observed at 40 meV in the normal state at optimal doping while the 41 meV spin resonance mode exists only below T_c [15]. The kink is sharp in the superconducting state of a deeply overdoped B12212 sample (Fig. 1e, consistent with data of [12]) while no spin resonance mode has been reported, or is expected to exist at this doping. In addition the kink seen in under-doped B12212 (Fig. 1d) is just as sharp as in the optimally doped case, while the neutron resonance peak is much broader [15]. Lastly, it is difficult

to account for the strong kink effect seen throughout the BZ from the spin mode since the mode's spectral weight is only 2% [16] as it may only cause a strong enough kink effect if the interaction with electrons is highly concentrated in k-space [17].

On the other hand, it has been argued that the bosonic renormalization effect may be reinterpreted as a result of a coupling to the half-breathing in-plane Cu-O bond-stretching phonon for nodal directions [6, 7] and the out-of-plane out-of-phase O buckling B_{1g} phonon for anti-nodal directions [13]. This re-interpretation has the clear advantage over the spin resonance in that it naturally explains why the band renormalization effect is observed under three circumstances: 1) in materials where no spin mode has been detected, 2) in the normal state, and 3) in the deeply overdoped region where the spin mode is neither expected nor observed. However, this interpretation also requires that the electron-phonon interaction be highly anisotropic and its impact on the electrons be strongly enhanced in the superconducting state. This is something one does not expect a priori.

We now show that the anisotropy of the electron-phonon interaction of these phonons, when formulated within the same framework as that used to explain phonon lineshape changes observed via Raman and neutron measurements [1, 2, 18, 19], explain the observed momentum and temperature dependence of the data, leading to unified understanding of band renormalizations. The electron-phonon interactions are very anisotropic as a consequence of the following four properties of the cuprates: 1) the symmetry of the phonon polarizations and electronic orbitals involved leading to highly anisotropic electron-phonon coupling matrix elements $g(k; q)$; 2) the kinematic constraint related to the anisotropy of the electronic band structure and the van Hove singularity (VHS); 3) the d-wave superconducting gap, and 4) the near degeneracy of energy scales of the B_{1g} phonon, the superconducting gap, and the VHS.

We consider a tight-binding three-band Hamiltonian modified by B_{1g} buckling vibrations as considered in Ref. [18] and in-plane breathing vibrations as considered in Ref. [20]:

$$\begin{aligned}
 H = & \sum_{\mathbf{n}} \sum_{\sigma} \epsilon_{\mathbf{n}} c_{\mathbf{n}\sigma}^\dagger c_{\mathbf{n}\sigma} + \sum_{\mathbf{n}, \mathbf{n}'} \sum_{\sigma} t_{\mathbf{n}, \mathbf{n}'} c_{\mathbf{n}\sigma}^\dagger c_{\mathbf{n}'\sigma} \\
 & + \sum_{\mathbf{n}} \sum_{\sigma} \left(\epsilon_{\mathbf{n}} + \epsilon_{\mathbf{n}}^0 + \epsilon_{\mathbf{n}}^0 \cos(\phi_{\mathbf{n}}) \right) a_{\mathbf{n}\sigma}^\dagger a_{\mathbf{n}\sigma} \\
 & + \sum_{\mathbf{n}, \mathbf{n}'} \sum_{\sigma} P_{\mathbf{n}, \mathbf{n}'} \left(Q_{\mathbf{n}, \mathbf{n}'} \cos(\phi_{\mathbf{n}}) \right) a_{\mathbf{n}\sigma}^\dagger a_{\mathbf{n}'\sigma} + \text{h.c.} \\
 & + \sum_{\mathbf{n}} \sum_{\sigma} P_{\mathbf{n}, \mathbf{n}}^0 \left(a_{\mathbf{n}\sigma}^\dagger a_{\mathbf{n}\sigma} + \text{h.c.} \right)
 \end{aligned} \quad (1)$$

with Cu-O hopping amplitude t , O-O amplitude t^0 , and

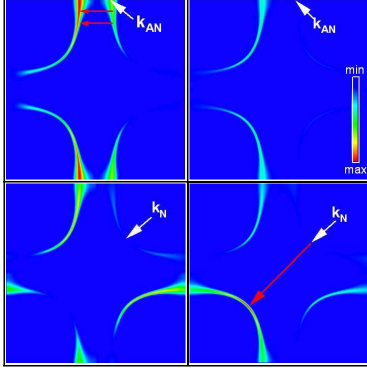


Fig. 3. Plots of the electron-phonon coupling $jg(k;q)$ for initial k and scattered $k^0 = k - q$ states on the Fermi surface for the buckling mode (left panels) and breathing mode (right panels) for initial fermion k at an anti-nodal (top panels) and nodal (bottom panels) point on the Fermi surface, as indicated by the arrows. The red/blue color indicates the maximum/minimum of the elph coupling vertex in the BZ for each phonon.

d_{BP} denoting the Cu and O site energies, respectively. Here $a_{x/y} = a_{x/y}^\dagger$; $a_{x/y}^\dagger$ annihilates, creates an electron in the O (Cu) orbital, respectively. The overlap factors Q_x, P_x ; and P_y, Q_y are given in our notation as $Q_x = Q_y = 1; P_x = P_y = 1; P_{x,y}^0 = 1; P_{x,y}^0 = 1$. For the half-breathing mode we consider only couplings $g_{\text{BP}} = g_{\text{BP}}(q)$ (with $l=q$ a length scale) arising from modulation of the covalent hopping amplitude t [20,21]. For the B_{1g} mode a coupling to linear order in the atomic displacements arises from a local c -axis oriented crystal field E_z which breaks the mirror plane symmetry of the Cu-O plane [18]. Such a field may be due to static buckling or different valences of ions on either side of the Cu-O plane, orthorhombic tilts of the octahedra, or may be generated dynamically.

The amplitudes of the tight-binding wavefunctions forming the anti-bonding band with energy dispersion $\epsilon(k)$ arising from Eq. 1 include the symmetry of the p_{d} wavefunctions of the Cu-O plane. The specific transformation is constructed from the projected part of the tight-binding wavefunctions $b_{\mathbf{k}} = b(\mathbf{k})d_{\mathbf{k}}$, and $a_{\mathbf{k}} = b(\mathbf{k})d_{\mathbf{k}}$,

$$b(\mathbf{k}) = \frac{1}{N(\mathbf{k})} [\epsilon^2(\mathbf{k}) - t^2(\mathbf{k})]; \quad (2)$$

$$x_{iy}(\mathbf{k}) = \frac{i}{N(\mathbf{k})} [(\mathbf{k})t_{iy}(\mathbf{k}) - t^0(\mathbf{k})t_{yx}(\mathbf{k})]; \quad (3)$$

with $N^2(\mathbf{k}) = [\epsilon^2(\mathbf{k}) - t^2(\mathbf{k})]^2 + [(\mathbf{k})t_{xy}(\mathbf{k}) - t^0(\mathbf{k})t_{yx}(\mathbf{k})]^2 + [(\mathbf{k})t_{yz}(\mathbf{k}) - t^0(\mathbf{k})t_{zy}(\mathbf{k})]^2$, $t(\mathbf{k}) = 2t \sin(k_x a/2)$; and $t^0(\mathbf{k}) = 4t^0 \sin(k_x a/2) \sin(k_y a/2)$. In particular if k resides on the Fermi surface, then

$$F_{xy}^S(\mathbf{k}) = \frac{j t^0(\mathbf{k}) j}{t^0(\mathbf{k})^2 + t_x(\mathbf{k})^2 + t_y(\mathbf{k})^2}; \quad (4)$$

$$F_{xy}^S(\mathbf{k}) = \frac{\text{isgn}[t^0(\mathbf{k})] t_{yx}(\mathbf{k})}{t^0(\mathbf{k})^2 + t_x(\mathbf{k})^2 + t_y(\mathbf{k})^2}; \quad (5)$$

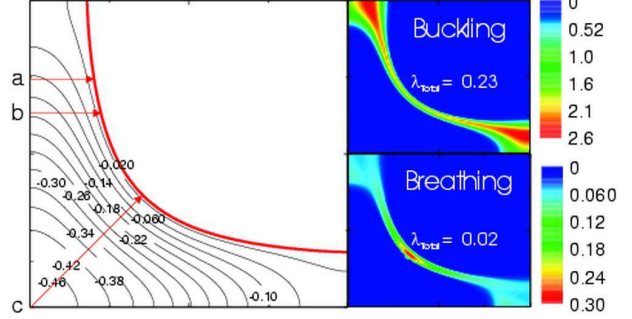


Fig. 4. Plots of the electron-phonon coupling λ_{ph} in the first quadrant of the BZ for the buckling mode (right top panel) and breathing mode (right bottom panel). The color scale is shown on the right for each phonon. The left panel shows energy contours for the band structure used [23].

The full anisotropy of the electron-phonon coupling comes from the projected wavefunctions in combination with the phonon eigenvectors: $H_{\text{el-ph}} = \frac{1}{N} \sum_{\mathbf{k}, \mathbf{q}} g(\mathbf{k}; \mathbf{q}) c_{\mathbf{k}}^\dagger c_{\mathbf{k}+\mathbf{q}} [a_{\mathbf{q}}^\dagger + a_{\mathbf{q}}]$. Neglecting the motion of the heavier Cu atoms compared to O in the phonon eigenvectors the form of the respective couplings can be compactly written as

$$g_{B_{1g}}(\mathbf{k}; \mathbf{q}) = e E_z \frac{S}{4M_{\text{O}} M(\mathbf{q}) B_{1g}} \quad (6)$$

$$g_{\text{br}}(\mathbf{k}; \mathbf{q}) = g_{\text{dp}} \frac{r}{2M_{\text{O}} \text{br}} \frac{x}{-x_{iy}} \quad (7)$$

with $M(\mathbf{q}) = [\cos^2(q_x a/2) + \cos^2(q_y a/2)]/2$ and $k^0 = k - q$. Here we have neglected an overall irrelevant phase factor. The anisotropy can be shown at small momentum transfers q where $g_{B_{1g}}(\mathbf{k}; q=0) = \cos(k_x a) \cos(k_y a)$, while $g_{\text{br}} = \sin(qa)$ for any k . Also for large momentum transfer $q = (\pi/a; \pi/a)$, $g_{B_{1g}}$ vanishes for all k while g_{br} has its maximum for k located on the nodal points of the Fermi surface. While this q -dependence has been the focus before in context with a $d_{x^2-y^2}$ pairing mechanism [22], the dependence on fermionic wavevector k has usually been overlooked. This strong momentum dependence of the B_{1g} coupling implies that resistivity measurements would be sensitive only to the weaker part of the electron-phonon coupling, in agreement with experiments. It is exactly this fermionic dependence which we feel is crucially needed to interpret ARPES data.

Fig 3 plots $jg(k;q)$ as a function of phonon scattered momentum q connecting initial k and nodal

an Einstein like break up into a band that follows the phonon dispersion, and one that follows the electronic one. In cut b, a weaker signature of coupling manifests itself in an s like renormalization of the bare band that traces the real part of the phonon self-energy, while in cut c, where the coupling to the B_{1g} phonon is weakest, the electron-phonon coupling manifests itself as a change in the velocity of the band. The agreement is very good, even for the large change in the electron-phonon coupling seen between cuts a and b, separated by only 1/10th of the BZ.

We now discuss the reason for the strong anisotropy as a result of a concurrence of symmetries, band structure, d wave energy gap, and energy scales in the electron-phonon problem. In the normal state, weak kinks are observed at both phonon frequencies, but more pronounced at 70 meV for cut c and at 36 meV for cut a, as expected from the anisotropic couplings shown in Fig. 3. However this is also a consequence of the energy scales of the phonon modes and the bottom of electronic band along the cut direction as shown in Fig. 4. Further towards the antinode, another interesting effect occurs. As one considers cuts closer to the BZ axis, the bottom of the band along the cut rises in energy and the breathing phonon mode lies below the bottom of the band for $(k_x = 0; k_y > 0.82 \text{ \AA}^{-1})$ and so the kink feature for this mode disappears. This is the usual effect of a Fano redistribution of spectral weight when a discrete excitation lies either within or outside of the band continuum [26]. This thus can be used to open "windows" to examine the coupling of electrons to discrete modes in general. Taken together, this naturally explains why the normal state nodal kink is near 70 meV [5,6,7,8,9] while the antinodal kink is near 40 meV [10,11,12,13].

In the superconducting state the bare band renormalizes downward in energy due to the opening of the gap and gives the strongest effect for the antinodal region where the gap is of the order of the saddle point energy. The B_{1g} coupling becomes dramatically enhanced by the opening of the gap at a frequency close to the frequency of the phonon itself, and leads to the dramatic renormalization of the phonon observed in Raman and neutron measurements [1]. Yet the breathing coupling does not vary dramatically as the large gap region is not weighted as heavily by the coupling constant. As a consequence, the B_{1g} mode dominates and clear kinks in the data are revealed at around 70 meV – the B_{1g} energy plus the gap. Indeed a much weaker kink at 105 meV from the breathing phonon shows at higher energies for the nodal cut but this kink becomes weaker away from nodal directions as the coupling and the band bottom along the cut moves below the phonon frequency so that the "energy window" closes.

Finally we plot in Fig. 6 the superconducting density of states $\rho(E) = -\text{Im} G_{11}(k; i\omega)$ calculated with the

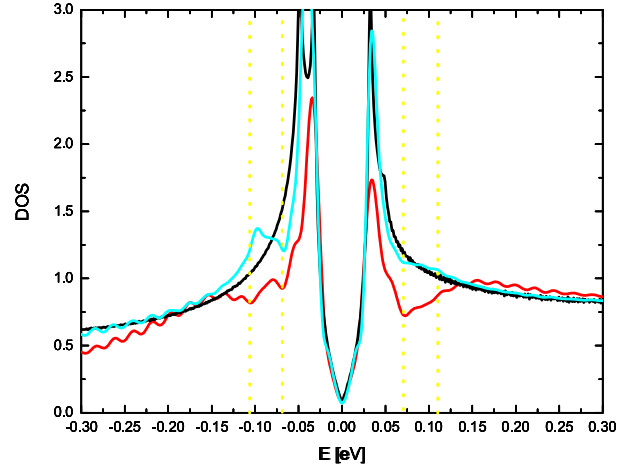


Fig. 6. Superconducting density of states calculated with the electron-phonon self energy for three different values of the electric field $E_z = 0$ (black), 1.85 (blue), and 3.2 (red), in units of $\text{eV}/\text{\AA}$, respectively. The yellow dashed lines indicate the energies $E_{B_{1g}} + 0$ and $E_{Br} + 0$.

electron-phonon contributions from both the breathing and B_{1g} phonons to the self energy determined via Eq. 9 for three different values of the B_{1g} coupling constant parametrized by the crystal field E_z . We have fixed the relative breathing coupling at $g_t = 2\sqrt{2}E_z$ as for ARPES. For these values of the coupling constants the structure in the DOS is determined largely by the antinodal couplings to the B_{1g} phonon. For the value of the coupling which fits the ARPES data well, the peak-dip-hump structure of the DOS (at values $E = 0; E_{B_{1g}} + 0$; and $E_{B_{1g}} + E_{VH}$, respectively) compares very well with the DOS determined via scanning tunnelling microscopy in Bi-2212 [27].

In summary, contrary to usual opinion of the role of anisotropy in electron-phonon coupling, the interplay of specific coupling mechanisms of electrons to the buckling and breathing phonons give a natural interpretation to the bosonic renormalization effects seen in ARPES in both the normal and superconducting states, and provides a framework to understand renormalizations as a function of doping.

Acknowledgments: ARPES data were collected at SSRL which is operated by DOE under contract DE-AC03-76SF00515. T.P.D. would like to acknowledge support from NSERC, PREA and the A. von Humboldt Foundation. The Stanford work is also supported by NSF grant DMR-0304981 and ONR grant N00014-01-1-0048.

References

- [1] B. Friedl et al., Phys. Rev. Lett. 65, 915 (1990); N. Pyka et al., Phys. Rev. Lett. 70, 1457 (1993); D. Reznik et al., Phys. Rev. Lett. 75, 2396 (1995).
- [2] S. L. Chaplot et al., Phys. Rev. B 52, 7230 (1995); R. J. McQueeney et al., Phys. Rev. Lett. 82, 628 (1999); 87, 077001 (2001); J.-H. Chung et al., Phys. Rev. B 67, 014517 (2003); S. Sugai et al., Phys. Rev. B 68, 184504 (2003).
- [3] J. P. Franck, in Physical Properties of High T_c Superconductors IV, edited by D. M. Ginsberg (World Scientific, Singapore, 1994), p. 189; M. K. Crawford, M. N. Kunchur, W. E. Farneth, E. M. McCarron, and S. J. Poon, Phys. Rev. B 41, 282 (1990).
- [4] R. Khasanov et al., Phys. Rev. Lett. 92, 057602 (2004); cond-mat/0404428.
- [5] P. V. Bogdanov et al., Phys. Rev. Lett. 85, 2581 (2000).
- [6] A. Lanzara et al., Nature 412, 510 (2001).
- [7] X. J. Zhou et al., Nature 423, 398 (2003).
- [8] A. Kaminski et al., Phys. Rev. Lett. 86, 1070 (2001).
- [9] P. D. Johnson et al., Phys. Rev. Lett. 87, 177007 (2001).
- [10] T. K. Kim et al., Phys. Rev. Lett. 91, 167002 (2003).
- [11] T. Sato et al., Phys. Rev. Lett. 91, 157003 (2003).
- [12] A. D. Gromko et al., Phys. Rev. B, 68, 174520 (2003).
- [13] T. Cuk et al., Phys. Rev. Lett. 93, 117003 (2004).
- [14] S. LaShell, E. Jensen, T. Balasubramanian Phys. Rev. B 61, 2371 (2000).
- [15] H. F. Fong Phys. Rev. Lett. 75, 316 (1995); P. Dai et al., Phys. Rev. B 63, 054525 (2001).
- [16] H.-Y. Kee, S. A. Kivelson, G. Aeppli, Phys. Rev. Lett. 88, 257002 (2002).
- [17] A. Abanov et al., Phys. Rev. Lett. 89, 177002 (2002).
- [18] M. Opel et al., Phys. Rev. B 60, 9836 (1999); T. P. Devereaux, A. V. Iosztek, and A. Zawadowski Phys. Rev. B 59, 14618 (1999); 51, 505 (1995).
- [19] T. P. Devereaux et al., Phys. Rev. Lett. 93, 117004 (2004).
- [20] S. Barišić, Phys. Rev. B 5, 932 (1972).
- [21] The coupling g_d arising from modulation of Cu site energies leads to a coupling which only depends on momentum transfers on not on fermion momentum [20].
- [22] D. J. Scalapino, J. Phys. Chem. Solids 56, 1669 (1995); A. Nazarenko and E. Dagotto, Phys. Rev. B 53, 2987 (1996); O. Jepsen et al., J. Phys. Chem. Solids 59, 1718 (1998); T. S. Nunner, J. Schmalian and K. H. Bennemann, Phys. Rev. B 59, 8859 (1999).
- [23] M. R. Norman et al., Phys. Rev. B 64, 184508 (2001). M. Eschrig and M. R. Norman, Phys. Rev. Lett. 85, 3261 (2000); Phys. Rev. B 67, 144503 (2003); A. V. Chubukov and M. R. Norman, cond-mat/0402304. cond-mat/0403766
- [24] O. Jepsen et al., J. Phys. Chem. Solids 59, 1718 (1998); O. K. Andersen et al., J. of Low Temp. Phys. 105, 285 (1996); S. Y. Savrasov and O. K. Andersen, Phys. Rev. Lett. 77, 4420 (1996).
- [25] A. W. Sandvik, D. J. Scalapino, N. E. Bickers, Phys. Rev. B 69, 094523 (2004).
- [26] U. Fano, Phys. Rev. 124, 1866 (1961).
- [27] E. W. Hudson, S. H. Pan, A. K. Gupta, K.-W. Ng, and J. C. Davis, Science 285, 88 (1999); J. F. Zasadzinski, L. Coey, P. Romano, and Z. Yusuf, Phys. Rev. B 68, 180504 (2003).